Research in
Astronomy and
Astrophysics

Photometric analysis of the eclipsing polar MN Hya

Qi-Shan Wang[1,2,3], Sheng-Bang Qian[1,2,3], Zhong-Tao Han[1,2,3], Miloslav Zejda[4],
Eduardo Fernández-Lajus[5,6] and Li-Ying Zhu[1,2,3]

[1] Yunnan Observatories, Chinese Academy of Sciences, Kunming 650216, China; *wangqs@ynao.ac.cn*

[2] Key Laboratory of the Structure and Evolution of Celestial Objects, Chinese Academy of Sciences, Kunming 650216, China

[3] University of Chinese Academy of Sciences, Beijing 100049, China

[4] Department of Theoretical Physics and Astrophysics, Masaryk University, Kotlárská 2, Brno 611 37, Czech Republic

[5] Facultad de Ciencias Astronómicas y Geofísicas, Universidad Nacional de La Plata, Paseo del Bosque s/n, 1900, La Plata, Pcia. Bs. As., Argentina

[6] Instituto de Astrofísica de La Plata (CCT La plata - CONICET/UNLP), Argentina

Abstract As an eclipsing polar with a 3.39 h orbital period, MN Hya was going through a state change when we observed it during 2009–2016. Ten new mid-eclipse times, along with others obtained from literature, allow us to give a new ephemeris. The residuals of a linear fit show that period decreased during the phase of state change, which means angular momentum was lost during this phase. The associated X-ray observation indicates the mass accretion rate was about $3.6 \times 10^{-9} \, M_\odot \, \mathrm{yr}^{-1}$. The period decrease indicates that at least 60% of mass being transferred from the secondary was lost, maybe in the form of spherically symmetric stellar wind. In the high state, the data show the intensity of flickering reduced when the system had a higher accretion rate, and that flickering sticks out with a primary timescale of about 2 min, which implies the position of the threading point was about 30 white dwarf radii above its surface. The trend of light curves for the system in its high state follows that of the low state for a large fraction of the phase interval from phase 0 to phase 0.4 since, starting at phase 0.4, the cyclotron feature is visible, and the primary intensity hump of the light curves near phase 0.7 when the system is in the high state did not appear on the curve when it was in the low state. Those facts contradict predictions of the two-pole model.

Key words: techniques: photometric — stars: cataclysmic variables: eclipsing polars — stars: individual (MN Hya)

1 INTRODUCTION

MN Hya was detected as the optical counterpart of the X-ray source RX J0929.1-2404 and identified as a polar due to its spectral characteristics (Sekiguchi et al. 1994). As one of the subtypes of cataclysmic variables (CVs), polars are interacting binaries in which mass transfers from a dwarf secondary star to the primary, a magnetic ($\sim 10 - 200 \, \mathrm{MG}$) white dwarf (WD), through Roche lobe overflow. The magnetic field is sufficiently high to prevent the formation of an accretion disc and channels the accretion stream at the threading point, then guides the flow plunging into the WD directly around the magnetic pole (Hellier 2001). If only one accretion region is visible, we call the behavior one-pole behavior. In contrast to two-pole behavior, two accretion regions appear alternatively. Because of variation in the mass transfer rate, polars switch irregularly between their high state and low state. In the high state, polars present fast light intensity variation which is known as flickering. Later,

several observations of MN Hya, including photometry, spectrometry, X-ray and polarimetry, led some authors to classify it as a two-pole system. The primary accretion pole, below the orbital plane, appears between phase $\sim 0.5 - 1$ and causes the intensity peak near phase 0.7 while the secondary accretion pole contributes all of its emission (Buckley et al. 1998b). MN Hya also shows a prominent pre-eclipse dip in X-rays around phase 0.9, but this is not detected in the optical passband with the same depth and phase interval (Buckley et al. 1998a). Moreover, MN Hya is an eclipsing system with a high orbital inclination of $\sim 75°$ (Buckley et al. 1998b). The eclipsing nature provides a good opportunity to ascertain its geometric structure and evolutionary state, and also to search for circumbinary planets. Since 2009, our group started to detect the secular evolution of CVs and the extrasolar planets around them by the eclipse timing method (e.g. Qian et al. 2009, 2010, 2011, 2015, 2016; Dai et al. 2009, 2010; Han et al. 2015, 2016, 2017a,b,c).

In this paper, we analyze the photometric observations of MN Hya. We give a revised ephemeris and find that the orbital period decreased during the state change. The light curve (LC) of the low state presents one hump near phase 0.2 and that of the high state shows obvious flickering. The paper is organized in the following way. In Section 2, observation of the datasets is described. A detailed analysis is provided in Section 3. Our main results are summarized in Section 4.

2 OBSERVATIONS

In this study, MN Hya started being observed on 2009 November 27 by using the 2.4 m telescope at the Lijiang observational station of Yunnan Observatories (YNAO). Later, this binary was monitored during 2012–2016 with the Danish 1.54-m Telescope at ESO in La Silla, Chile. MN Hya was detected photometrically 12 times, mostly with no filter used, apart from one observation through V filter on 2016 January 17. The CCD images were reduced with the help of the aperture photometry package in IRAF (Tody 1993). Nearby non-variable stars were chosen as comparison star and check star (the stars marked C and B respectively in figure 2 of Sekiguchi et al. (1994)), so two sets of different magnitudes for each observation, i.e. the magnitudes of the object and the companion star with respect to that of companion star and check star respectively, were obtained and used for analysis of the characteristics of the LC associated with the object. An overview of the observation of MN Hya is given in

Table 1. The table lists information about an observation ID used in this paper, information about the observation, state of the object, time resolution, the telescope and filter used, and total phase coverage.

Figure 1 displays all LCs obtained in 2009–2016. We were fortunate to detect the process of state change which enables us to examine characteristics of this phase.

3 ANALYSIS

3.1 Period Change

From our photometric observations that included 10 mid-eclipse times, the average of eclipse ingress and egress, were obtained, and a linear least-squares fit to the timings gives the following eclipsing ephemeris

$$\begin{aligned} \text{HJD}_{\text{min}} =& 2457458.62831(4) \\ &+ 0.1412437990(31)E. \end{aligned} \tag{1}$$

Figure 2 shows the residual ($O - C$, observed minus calculated) times of the linear fit. The $O - C$ curve indicates that the orbital period decreased during the state change. Because the mid-eclipse time is that of the occultation of the primary by the secondary (Schmidt & Stockman 2001) which cannot be affected by shift of the accretion spot due to variation of accretion rate, the $O - C$ curve of the system will provide information on orbital evolution. The new data have higher precision, making it possible to analyze the orbital variation. The period decreased as $-2.4 \times 10^{-12}\,\text{d cyc}^{-1}$ with an error of $0.7 \times 10^{-12}\,\text{d cyc}^{-1}$. If angular momentum is conserved, the orbital period increases when mass transfers from the less massive secondary to the more massive primary white dwarf (WD), which makes the $O - C$ curve form a parabola with a positive quadratic term. So, we infer that mass transfers from the secondary to the primary, accompanied by intense mass loss which carries angular momentum from the system and decreases the orbital period.

In order to estimate the mass loss fraction from the system during the high state, we need to know the accretion luminosity. The period ($P \approx 3.39\,\text{h}$) implies that the secondary has mass $M_2 = 0.22\,M_\odot$ and radius $R_2 = 0.32\,R_\odot$ (Knigge 2006). Considering inclination of the system, $i = 75°$, and phase width of eclipse, about 0.036, we deduce the mass ratio ($q = M_2/M_1$) to be about 0.38 (Horne 1985), which implies the primary has mass $M_1 = 0.58\,M_\odot$ and radius $R_1 = 0.88 \times 10^9\,\text{cm}$ (Nauenberg 1972). The $0.1 - 2.4\,\text{keV}$ luminosity

Table 1 Log of photometric observations for MN Hya. The meanings of the entries are given in the main text.

Obs-ID	Date	Accretion state	Resolution (s)	Telescope (m)	Filter	Phase coverage[a]
Run0	20091127	intermediate	23	2.4	N	0.72–1.31
Run1	20091128	intermediate	23	2.4	N	0.84–1.35
Run2	20100115	intermediate	28	2.4	N	0.77–1.31
Run3	20101227	intermediate	40	2.4	N	0.85–1.15
Run4	20101230	intermediate	40	2.4	N	0.84–1.09
Run5	20121225	high	16	1.54	N	0.82–1.82
Run6	20130406	high	16	1.54	N	0.18–1.43
Run7	20131223	high	14	1.54	N	0.89–1.08
Run8	20150129	high	16	1.54	N	0.69–1.43
Run9	20160101	high	21	1.54	N	0.03–1.08
Run10	20160117	high	22	1.54	V	0.17–1.38
Run11	20160310	low	17	1.54	N	0.89–1.95

Notes: [a] Phase is calculated according to the ephemeris of Eq. (1).

is about $9 \times 10^{32} \, \mathrm{erg \, s^{-1}}$ (Ramsay & Wheatley 1998). With the addition of soft X-ray excess ($\frac{L_{\mathrm{bb}}}{L_{\mathrm{brems}}+L_{\mathrm{cycs}}}$) $\sim$ 10 (Buckley et al. 1998a) and assuming

$$L_{\mathrm{brems}} = L_{\mathrm{cycs}},$$

we derive that the luminosity of accretion is about

$$L_{\mathrm{acc}} = 2 \times 10^{34} \, \mathrm{erg \, s^{-1}},$$

which yields the mass accretion rate of

$$\dot{M}_1 = 3.6 \times 10^{-9} \, M_\odot \, \mathrm{yr^{-1}}.$$

Combining

$$\frac{\dot{J}}{J} = \frac{\dot{M}_1}{M_1} + \frac{\dot{M}_2}{M_2} - \frac{1}{2}\frac{\dot{M}}{M} + \frac{1}{2}\frac{\dot{a}}{a}, \quad (2)$$

with Kepler's law and assuming mass loss rate

$$\dot{M} = \alpha \dot{M}_2,$$

we can write

$$\frac{\dot{J}}{J} = \left(1 + \frac{1}{q(\alpha-1)} - \frac{1}{3}\frac{\alpha}{(1+q)(\alpha-1)}\right)$$
$$\frac{\dot{M}_1}{M_1} + \frac{1}{3}\frac{\dot{P}}{P}, \quad (3)$$

where $M = M_1 + M_2$ is the mass of the system and $J = M_1 M_2 \sqrt{Ga/M}$ is the angular momentum of the system. The $\dot{J}/J$ term consists of the angular momentum loss due to mass lost from the system and redistribution of mass between two components. The first factor (denoted as the loss-term) can be expressed by

$$\left(\frac{\dot{J}}{J}\right)_{\mathrm{loss}} = \frac{1+q}{q}\frac{\alpha}{\alpha-1}\frac{\dot{M}_1}{M_1}\left(\frac{r_{\mathrm{de}}}{a}\right)^2, \quad (4)$$

which has the effective decoupling position r_{de}

$$\left(\frac{r_{\mathrm{de}}}{a}\right)^2 = \left(\frac{r_1}{a}\right)^2 + \left(\frac{r_2}{a}\right)^2 + 2\frac{r_1}{a}\frac{r_2}{a}\cos\Delta\theta, \quad (5)$$

where r_1 is the line length from one component to the center of mass (COM) for the system, r_2 is that from the decoupling point to this component and $\Delta\theta$ is the angle between the two lines assuming 0 degree corresponds to the decoupling point in the opposite direction to COM. The second factor (denoted as the syn-term) can be calculated using

$$\left(\frac{\dot{J}}{J}\right)_{\mathrm{syn}} = \frac{2\pi\dot{M}_1 a^2}{JP}\left[\left(\frac{l_1}{a}\right)^2 - \left(\frac{q}{1+q}\right)^2\right]$$
$$= \frac{1+q}{q}\frac{\dot{M}_1}{M_1}\left[\left(\frac{l_1}{a}\right)^2 - \left(\frac{q}{1+q}\right)^2\right], \quad (6)$$

with

$$l_1 = a(0.5 - 0.227\log q) - \frac{qa}{1+q}, \quad (7)$$

giving the distance of the Lagrangian radius (R_{L1}, Plavec & Kratochvil 1964) to COM.

Substituting the parameters into the equations above produces

$$\left(\frac{r_{\mathrm{de}}}{a}\right)^2 \sim \frac{1.12}{\alpha} - 0.46. \quad (8)$$

The constraint $\alpha < 1$ gives $r_{\mathrm{de}}/a > 0.81$ which implies mass is lost from the secondary. Note that the shortest length scale from the decoupling point to the COM only depends on the mass ratio, i.e., it is independent of the variation of period, mass accretion rate or other physical parameters. The maximal length scale of the system is about $1.2a$, corresponding to the distance from Lagrangian point L2 to COM, demonstrating that the
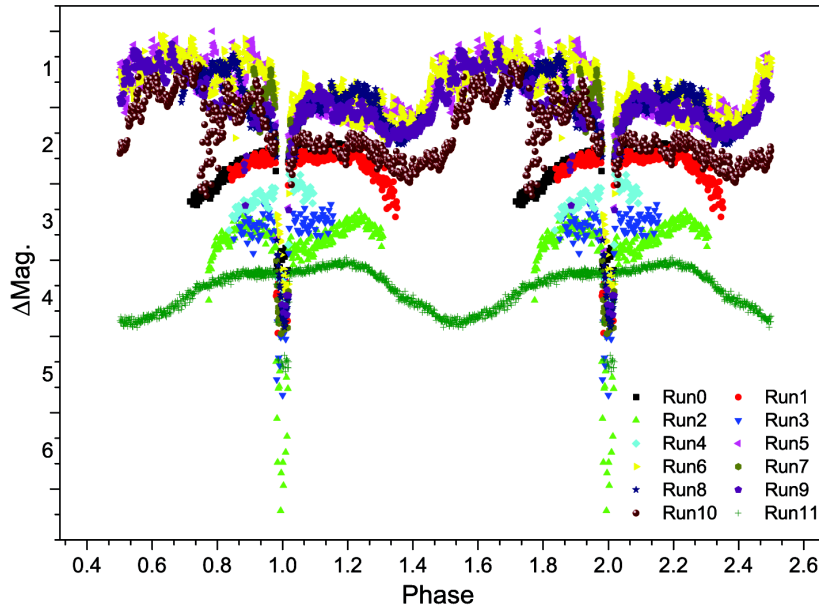
Fig. 1 All LCs detected during 2009–2016. The ordinate is the differential magnitude of the target star with respect to the comparison star. The labels indicate the observation IDs used in this paper. More information is given in Table 1.
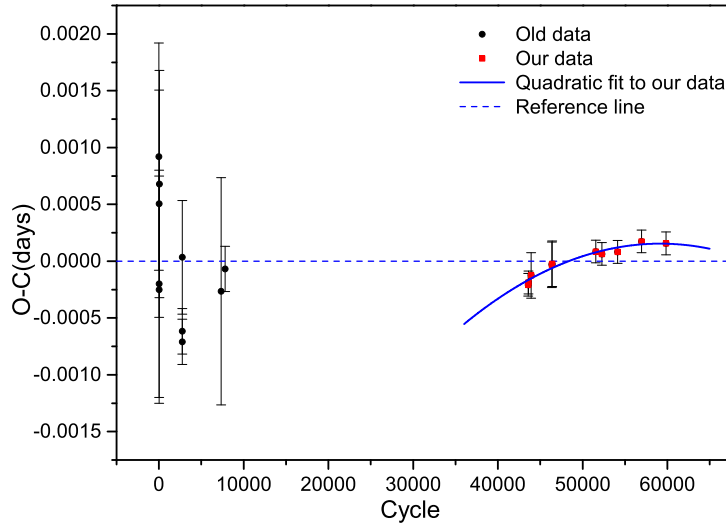

Fig. 2 The residuals of the linear fit to the mid-eclipse times with the reference line for convenience. The new data overlaid by a fitted parabola show a period decrease.

minimal mass loss fraction α is about 60%, and indicating that mass transfer rate from the secondary is at least about $6 \times 10^{-9}\ M_\odot\,\mathrm{yr}^{-1}$. The Alfvén radius, considering the equivalence of ram pressure from the flow and magnetic pressure from the field, is described by (Frank et al. 2002)

$$r_\mathrm{A} = 2.9 \times 10^8 M_1^{-1/7} R_6^{10/7} L_{37}^{-2/7} B_{12}^{4/7}, \qquad (9)$$

from which we can estimate the Alfvén radius r_A to be about $1.02a$. The magnetosphere centered on the primary can cover about 42% of the surface area of the secondary, which can cause a mass loss fraction of about 58% if the secondary ejects matter symmetrically, such as with an intense global wind. This kind of activity can produce a mass loss fraction of about 58%, which is very close to

the mass loss fraction $\alpha \sim 60\%$ if mass is lost through the L_2. Regardless, we can see that the mass loss fraction is very large and any model not taking mass loss into account should be unrealistic.

3.2 Characteristics of the LC

Now we describe characteristics of the LC more carefully and analyze the reasons for corresponding variation. Analysis of the rapid light intensity is given in Subsection 3.3.

(a) Figure 3 shows details of the high-state LCs. Some LCs display a conspicuous pre-eclipse light decrease, such as near phase 0.85 in Run6 and phase 0.89 in Run9. This behavior is reminiscent of an X-ray pre-eclipse dip but with less phase extension. The eclipse profile also varies significantly, especially that of Run8. The intensity during the eclipse of Run8, after a possibly flat base ahead of a slow decrease, rises slowly, which indicates that some part of the accretion flow became brighter and the system had a higher mass transfer rate. The smooth increase and decrease of light during the eclipse mean that the fast light intensity variation is not due to accretion flow. All of these changes presented in LCs reflect a significant variation of the mass accretion rate during the high state.

(b) In Figure 4, all data are shifted by the average magnitude between phase 0.07–0.09. Referring to Figure 1, we can find most high-state LCs follow the LC of Run11 very well during phase $\sim 0- \sim 0.4$, except those of Run5 and Run6. The reason for their deviation, we think, is due to instability of the system at the beginning of the high state, such as Run2 which gives the light intensity variation of the system at the start of leaving the low state. The large phase interval $\phi_f \sim 0.4$ suggests that the only reasonable source giving rise to the hump near phase 0.2 is the WD itself. So from the shifting value of LCs, we can deduce the optical temperature relation of the WD between the low and high states. Assuming blackbody radiation and using the magnitude formula, we can find

$$
\begin{aligned}
m_{\mathrm{H}} - m_{\mathrm{L}} &= -2.5 \log \frac{f_{\mathrm{H}}}{f_{\mathrm{L}}} \\
&= -2.5 \log \left(\frac{S_{\mathrm{H}} \bar{T}_{\mathrm{H}}^4}{S_{\mathrm{L}} \bar{T}_{\mathrm{L}}^4} \right),
\end{aligned}
\tag{10}
$$

where m, S and $\bar{T}$ are respectively the magnitude, projected surface area and mean temperature of the system, and L and H denote the low and high states respectively.

Considering the dominant optical radiation from the WD and its spherical symmetry during phase 0–0.4, and that the projected surface area is constant at a certain phase, we find

$$
\begin{aligned}
m_{\mathrm{H}} &= m_{\mathrm{L}} - 10 \log \left(\frac{\bar{T}_{\mathrm{H}}}{\bar{T}_{\mathrm{L}}} \right) \\
&= m_{\mathrm{L}} + \Delta \mathrm{Mag},
\end{aligned}
\tag{11}
$$

where $\Delta \mathrm{Mag}$ is the amount of translation for high-state LCs to overlap that of Run11. With $\Delta \mathrm{Mag} = -2.21$, we find $\bar{T}_2 \approx 1.66 \bar{T}_1$. If the temperature of the WD in the low state is about 9000 K (Ramsay et al. 2004), we deduce the optical temperature of the WD in the high state is about 15 000 K. Also as shown in the inset graph of Figure 4, LCs of the high state deviate from the behavior shown by Run11 near phase 0.4, since the cyclotron features are visible (Ramsay & Wheatley 1998) and the accretion region appears there. Both the large ϕ_f during phase 0–0.4 and the visible cyclotron features during phase 0.4–1 suggest that it is a one-pole system.

3.3 Flickering

Even though the LCs from the intermediate state have less phase coverage than others, we can find the flickering only becomes apparent in the high state, which indicates that the flickering accompanies a high accretion rate and reminds us that transfer of material from the secondary is turbulent. In order to elucidate characteristics of the optical flickering of MN Hya, we analyze the spectrum of the LCs with enough phase coverage, the timescale of light intensity variation and the magnitude of the flickering in different parts of these LCs.

The data from each run were subjected to period searches using a discrete Fourier transform (DFT) and the phase dispersion minimization (PDM) method (see Stellingwerf 1978, or Dai et al. 2016, 2017 as reference). Figure 5 shows the spectrogram of the time series from Run6 as determined by DFT. The dominant peak corresponds to the time interval of the data and others with amplitude greater than 0.05 are the harmonics of this time. The PDM method provides a similar result. This result confirms that the rapid time variation is random, which is the same characteristic as exhibited by associated X-ray observations (Buckley et al. 1998a). However, the system shows obvious evidence for brightness variations on timescale of minutes, which might be explained in that there are some oscillations that last for only few phase

Table 2 All Mid-eclipse Times of MN Hya

Min. (HJD)	Cycle	Error (d)	Calculated	$O - C$ (d)	Reference
2449007.58900	0	0.001	2449007.58808	0.00092	[1]
2449009.42400	13	0.001	2449009.42425	–0.00025	[1]
2449009.56600	14	0.001	2449009.56549	0.00051	[1]
2449010.55400	21	0.001	2449010.55420	–0.00020	[1]
2449013.52100	42	0.001	2449013.52032	0.00068	[1]
2449397.42100	2760	0.0005	2449397.42097	0.00003	[1]
2449397.56150	2761	0.0002	2449397.56221	–0.00071	[1]
2449398.55030	2768	0.0002	2449398.55092	–0.00062	[1]
2450045.02352	7345	0.0010	2450045.02378	–0.00026	[1]
2450109.85462	7804	0.0002	2450109.85469	–0.00007	[1]
2455163.41637	43583	0.0001	2455163.41657	–0.00021	[2]
2455164.40509	43590	0.0001	2455164.40528	–0.00019	[2]
2455212.28680	43929	0.0002	2455212.28693	–0.00013	[2]
2455558.33420	46379	0.0002	2455558.33424	–0.00003	[2]
2455561.30033	46400	0.0002	2455561.30036	–0.00002	[2]
2456287.71730	51543	0.0001	2456287.71721	0.00008	[2]
2456389.69530	52265	0.0001	2456389.69524	0.00006	[2]
2456650.85510	54114	0.0001	2456650.85502	0.00008	[2]
2457052.83505	56960	0.0001	2457052.83487	0.00017	[2]
2457458.62847	59833	0.0001	2457458.62831	0.00016	[2]

Notes: [1] Sekiguchi et al. (1994); [2] Our observations.

intervals and then die away, to be replaced by other oscillations with a different period or at a different phase.

In order to find the characteristic timescale, we need to count the number of different timescales. The method employed to deal with the data is described below. First, in order to reduce the effect of variation of atmospheric seeing which can cause saw-toothed variation in an adjacent sequence, we use moving average with three points to smooth the raw data from each run; we then mark all the local extrema (maxima and minima), with which we give the histogram of the timescales between extrema that have the same type. As shown in Figure 6, we find the dominant variation timescale is about 2 min, which is a typical timescale in other X-ray systems, such as EF Eri (Patterson et al. 1981) (period 6 min), VV Pup (Maraschi et al. 1984) (period 3 min) and ST LMi (Beuermann & Stella 1985) (period 1 min). If these variations occur at the threading point where the matter is channeled by the magnetic field, the timescale for the Alfvén wave caused by unstable accretion to cross the magnetosphere is

$$P_{\text{ins}}(r) = 2 \times 10^{-3} r_8^{11/4} L_{34}^{1/2} f_{-2}^{-1/2} M_1^{-3/4}$$
$$\times R_8^{-3/4} B_7^{-1} \text{s}, \qquad (12)$$

where r_8 is the radius (in units of 10^8 cm, denoted as r_t below) of the threading point, L_{34} is the luminosity

in units of $10^{34}\,\text{erg\,s}^{-1}$, f is the fraction of the stellar surface where the accretion matter flows, M_1 is the WD mass in units of solar masses, R_8 is the radius of the WD in units of 10^8 cm and B_7 is the surface magnetic field strength in units of 10^{12} G. Adopting $f \approx 0.004$ (Schmidt & Stockman 2001), $B = 40$ MG (Buckley et al. 1998b) and other parameters mentioned earlier, we find r_t estimated for the timescale of 2 min to be 2.8×10^{10} cm or $30\,R_1$ ($0.62\,R_{L1}$). Comparing with the Alfvén radius, this length scale is much smaller, but is similar to that of AR UMa ($r_t \approx 0.6 - 0.7 R_{L1}$) as shown in Doppler tomograms (Hoard 1999), although the latter system has the highest magnetic field. If the optical flickering is caused by wobbling of the threading point, the impact of the magnetic field strength on its position is very little.

In order to quantify the flickering intensity, we remove the trend from the raw data using a 30 point moving average method and calculate the standard deviation of the detrended data as the flickering intensity.

Table 3 shows the flickering intensity corresponding to different phase intervals, considering the two-pole model where Source1, Source2 and Total represent phases 0.03–0.4, 0.4–0.97 and all phase coverage, respectively. From this table, we can find the flickering in-
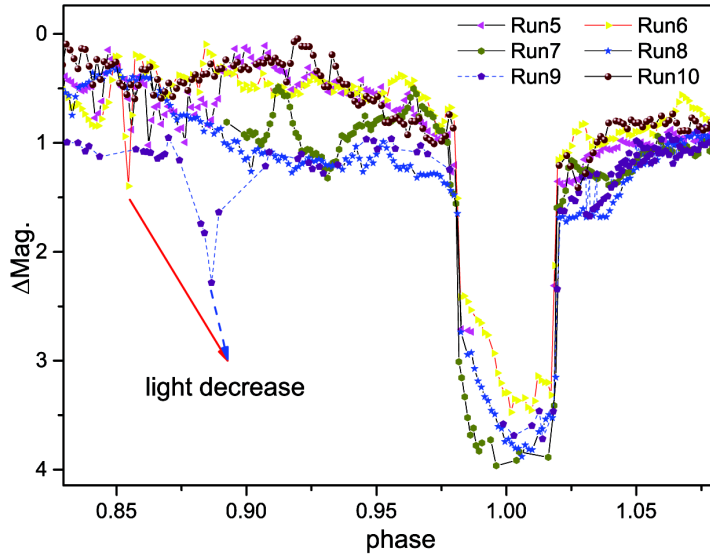
Fig. 3 A detailed plot of high-state LCs. The *arrows* indicate the position of the pre-eclipse light decrease.
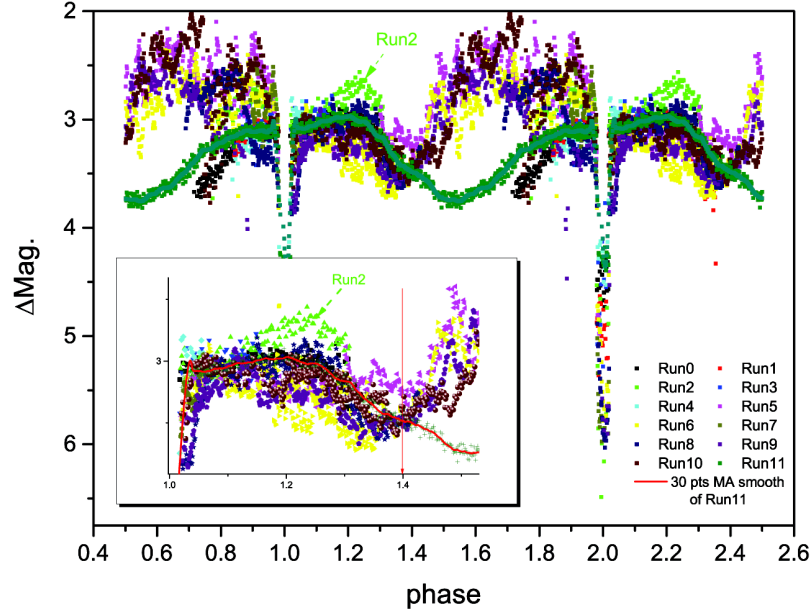

Fig. 4 All LCs shifted by the average magnitude between 0.07–0.09. The inset graph shows the outline of LCs during phase 0–0.5 with the vertical line indicating the phase at which the deviation starts.

Table 3 The flickering intensity of different parts, given in this table, is the standard deviation of the detrended data from the whole phase, phase $\sim 0.03 - 0.4$ and phase $\sim 0.4 - 0.97$, which are denoted as Total, Source1 and Source2, respectively.

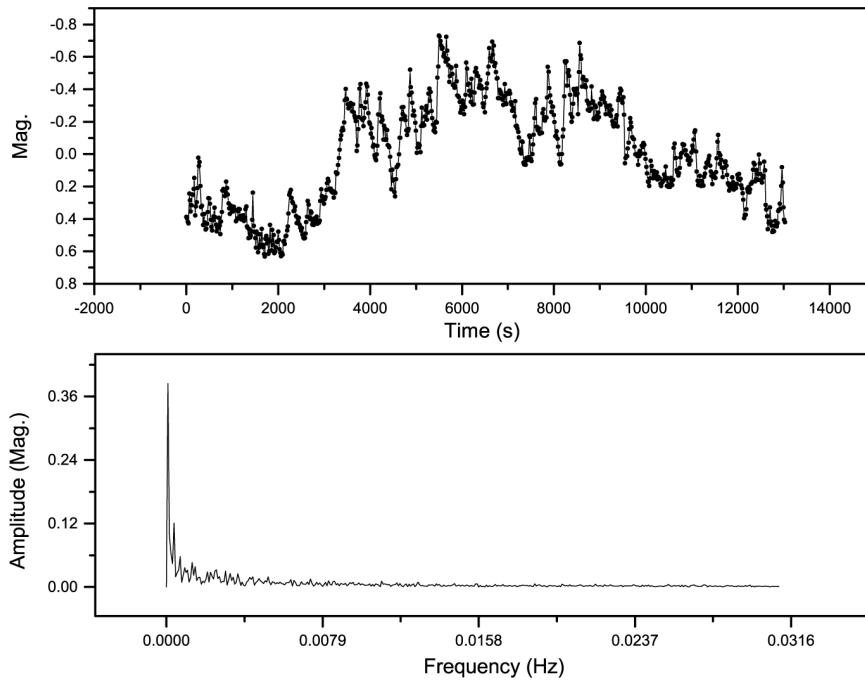| Source	Data					
	Run5	Run6	Run8	Run9	Run10	Run11
	Intensity (mag)					
Total	0.117	0.104	0.065	0.085	0.142	0.033
Source1	0.072	0.082	0.058	0.063	0.063	0.029
Source2	0.137	0.121	0.072	0.100	0.181	0.035

Fig. 5 The upper panel shows the time series of Run6 and the lower panel displays its spectrogram as determined by DFT. The dominant peak corresponds to the time interval of the data.
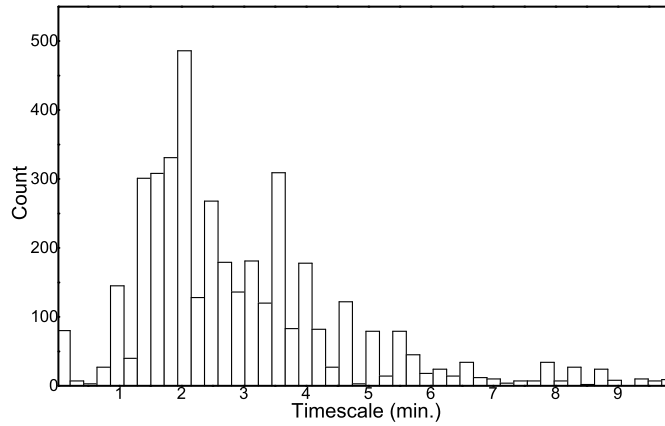

Fig. 6 Histogram of the variation timescales of all data. The dominant timescale is about 2 min.

tensity of Source1 is less than that of Source2 and that the flickering intensity reduces when the high-state system has a higher accretion rate, such as during Run8.

4 DISCUSSION AND SUMMARY

From the discovery mentioned above, we can describe the mass transfer process in MN Hya. The magnetosphere covers 42% of the surface area of the secondary.

Convection of the secondary can entangle the magnetic field which will be wound up, increasing the associated tension and stored energy until it reconnects to dissipate energy and cast matter globally, maybe in the form of intense stellar wind. This kind of matter with high velocity will pass through the Alfvén radius freely. When the matter flow reaches the threading point which has height of $\sim 30R_1$ above the surface of the WD, it will

be threaded by the magnetic field. As the system is in the high state, the accretion rate still varies which can trigger instability of the accretion column, and then an Alfvén wave will arise from the column and travel through accretion stream to the threading point. This wave causes instability in the threading point whose wobbling could modulate the mass accretion rate then give rise to fluctuation which causes the flickering.

In summary, the optical observations of the eclipsing polar MN Hya for 12 times during 2010–2016, with the addition of other observations, enable us to arrive at the following results:

(1) A revised ephemeris is given based on 10 more mid-eclipse times, along with others obtained from literature and the quadratic fit to new data, indicating the period decreased during the state change as $-2.4 \times 10^{-12}\,\mathrm{d\,cyc^{-1}}$, which cannot be explained if angular momentum is conserved. The X-ray observation by other authors implies the accretion rate is about $3.6 \times 10^{-9}\,M_\odot\,\mathrm{yr^{-1}}$ during the high state. These properties indicate the minimal distance of the decoupling point to the COM is about $0.81a$, which implies mass is lost from the secondary. The magnetosphere covers about 42% of the surface area of the secondary, which can cause a mass loss fraction of 58% if the secondary goes through an intense global stellar wind. This kind of mass loss fraction is very close to that deduced from losing mass through L2. The mass loss fraction is at least about 60%, so any model not taking the effect of mass loss into account should be unrealistic.

(2) The primary timescale of the flickering is about $2\,\mathrm{min}$, which implies the threading point is about $30R_1$ above the surface of the WD. In the high state, flickering is apparent, and originates from modulation of the accretion rate due to wobbling of the threading point; the data show the intensity of flickering reduces when the system has an increasing accretion rate.

(3) In the frame of the two-pole model, the dominant accretion region is nearly face on to us near phase 0.7. Considering the continuing mass transfer during the low state, this model predicts that the low-state LC should exhibit an intensity hump near phase 0.7, which contradicts the observation. The high-state LCs follow the shifting low-state LCs from phase 0 to phase 0.4; such a large fraction of phase indicates the hump near phase 0.2 is caused by the WD itself

rather than a tiny accretion region, which also does not conform to the two-pole model. These two facts make the two-pole model less convincing.

References

Beuermann, K., & Stella, L. 1985, Space Sci. Rev., 40, 139

Buckley, D. A. H., Barrett, P. E., Haberl, F., & Sekiguchi, K. 1998a, MNRAS, 299, 998

Buckley, D. A. H., Ferrario, L., Wickramasinghe, D. T., & Bailey, J. A. 1998b, MNRAS, 295, 899

Dai, Z.-B., Qian, S.-B., Fernández Lajús, E., & Baume, G. L. 2010, MNRAS, 409, 1195

Dai, Z., Qian, S., & Fernández Lajús, E. 2009, ApJ, 703, 109

Dai, Z., Szkody, P., Garnavich, P. M., & Kennedy, M. 2016, AJ, 152, 5

Dai, Z., Szkody, P., Taani, A., Garnavich, P. M., & Kennedy, M. 2017, A&A, 606, A45

Frank, J., King, A., & Raine, D. J. 2002, Accretion Power in Astrophysics: Third Edition (Cambridge: Cambridge University Press), 398

Han, Z.-T., Qian, S.-B., Fernández Lajús, E., Liao, W.-P., & Zhang, J. 2015, New Astron., 34, 1

Han, Z.-T., Qian, S.-B., Irina, V., & Zhu, L.-Y. 2017a, AJ, 153, 238

Han, Z.-T., Qian, S.-B., Voloshina, I., et al. 2016, RAA (Research in Astronomy and Astrophysics), 16, 156

Han, Z.-t., Qian, S.-b., Voloshina, I., & Zhu, L.-Y. 2017b, Ap&SS, 362, 109

Han, Z.-T., Qian, S.-B., Voloshina, I., & Zhu, L.-Y. 2017c, New Astron., 56, 22

Hellier, C. 2001, Cataclysmic Variable Stars (Springer)

Hoard, D. W. 1999, in Astronomical Society of the Pacific Conference Series, 157, Annapolis Workshop on Magnetic Cataclysmic Variables, ed. C. Hellier & K. Mukai, 201

Horne, K. 1985, MNRAS, 213, 129

Knigge, C. 2006, MNRAS, 373, 484

Maraschi, L., Beuermann, K., Bonnet-Bidaud, J. M., et al. 1984, in ESA Special Publication, 218, Fourth European IUE Conference, ed. E. Rolfe

Nauenberg, M. 1972, ApJ, 175, 417

Patterson, J., McGraw, J. T., Coleman, L., & Africano, J. L. 1981, ApJ, 248, 1067

Plavec, M., & Kratochvil, P. 1964, Bulletin of the Astronomical Institutes of Czechoslovakia, 15, 165

Qian, S. B., Han, Z. T., Fernández Lajús, E., et al. 2015, ApJS, 221, 17

Qian, S.-B., Liao, W.-P., Zhu, L.-Y., & Dai, Z.-B. 2010, ApJ, 708, L66

Qian, S. B., Soonthornthum, B., Dai, Z. B., et al. 2009, in Astronomical Society of the Pacific Conference Series, 404, The Eighth Pacific Rim Conference on Stellar Astrophysics:

A Tribute to Kam-Ching Leung, eds. S. J. Murphy & M. S. Bessell, 248

Qian, S.-B., Liu, L., Liao, W.-P., et al. 2011, MNRAS, 414, L16

Qian, S.-B., Han, Z.-T., Soonthornthum, B., et al. 2016, ApJ, 817, 151

Ramsay, G., Cropper, M., Wu, K., et al. 2004, MNRAS, 350, 1373

Ramsay, G., & Wheatley, P. J. 1998, MNRAS, 301, 95

Schmidt, G. D., & Stockman, H. S. 2001, ApJ, 548, 410

Sekiguchi, K., Nakada, Y., & Bassett, B. 1994, MNRAS, 266, L51

Stellingwerf, R. F. 1978, ApJ, 224, 953

Tody, D. 1993, in Astronomical Society of the Pacific Conference Series, 52, Astronomical Data Analysis Software and Systems II, eds. R. J. Hanisch, R. J. V. Brissenden, & J. Barnes, 173